Radiative and Dynamical Feedbacks Over the Equatorial Cold-Tongue: Results from Nine Atmospheric GCMs

D.-Z. Sun and T. Zhang
Climate Diagnostics Center, NOAA-CIRES

C. Covey and S.A. Klein
Lawrence Livermore National Laboratory

W.D. Collins, J. J. Hack, J.T. Kiehl, and G.A. Meehl
National Center For Atmospheric Research

I. M. Held
Geophysical Fluid Dynamics Laboratory, NOAA

M. Suarez
National Aronics and Space Administration

November 22, 2005

(Submitted to J. Climate)

Abstract

The equatorial Pacific is a region with strong negative feedbacks. Yet coupled general circulation models (GCMs) have exhibited a propensity to develop a significant SST bias in that region, suggesting an unrealistic sensitivity in the coupled models to small energy flux errors that inevitably occur in the individual model components. Could this "hypersensitivity" exhibited in a coupled model be due to an underestimate of the strength of the negative feedbacks in this region? With this suspicion, the feedbacks in the equatorial Pacific in nine atmospheric GCMs (AGCMs) have been quantified using the interannual variations in that region and compared with the corresponding calculations from the observations. The nine AGCMs are: the NCAR Community Climate Model Version 1 (CAM1), the NCAR Community Climate Model Version 2 (CAM2), the NCAR Community Climate Model Version 3 (CAM3), the NCAR CAM3 at T85 resolution, the NASA Seasonal-to-Interannual Prediction Project (NSIPP) Atmospheric Model, the Hadley Centre Model (HadAM3), the French IPSL Model (LMDZ4), the GFDL AM2p10, and the GFDL AM2p12. All the corresponding coupled runs of these nine AGCMs have an excessive cold-tongue in the equatorial Pacific.

The net atmospheric feedback over the equatorial Pacific in the two GFDL models is found to be comparable to the observed value. All other models are found to have a weaker negative net feedback from the atmosphere—a weaker regulating effect on the underlying SST than the real atmosphere. Except for the French model, a weaker negative feedback from the cloud albedo and a weaker negative feedback from the atmospheric transport are the two leading contributors to the weaker regulating effect from the atmosphere. The underestimate of the strength of the negative feedbacks by the models is apparently linked to an underestimate of the equatorial precipitation response. All models have a stronger water vapor feedback than that indicated in ERBE observations. These results confirm the suspicion that an underestimate of the regulatory effect from the atmosphere over the equatorial Pacific region is a prevalent problem. The results also suggest, however, that a weaker regulatory effect from the atmosphere is unlikely solely responsible for the "hypersensitivity" in all models. The need to validate the feedbacks from the ocean transport is therefore highlighted.

1.Introduction

The equatorial Pacific is a region with strong negative feedbacks. Ramanathan and Collins (1991) first observed that a SST anomaly in the central Pacific triggers a negative response from the short-wave forcing of clouds—deep clouds reflect more (less) solar radiation back to space in response to a positive (negative) SST changes. They even postulated that this negative feedback of cloud albedo may be a "thermostat" of the tropics. Subsequent studies point out the importance of the feedbacks from the atmospheric and oceanic dynamics (Fu et al 1990, Wallace 1992, Pierrehumert 1995, Sun and Liu 1996). In an attempt to assess the relative importance of the cloud albedo feedback and the feedback from dynamics, Sun and Trenberth (1998) used the best data available and quantified the changes in the heat transport in the atmosphere and in the ocean associated with the 1986-87 El Niño warming in addition to calculating the changes in the radiative fluxes. The results show that the negative feedback from the cloud albedo is actually a smaller player compared to the other two negative feedbacks in the equatorial Pacific region, namely the feedback from the heat transport by the atmospheric circulation and the feedback from the poleward heat transport by the ocean circulation. The negative feedback from the poleward ocean heat transport is found to be twice as strong as the negative feedback from the atmospheric transport. The latter is in turn twice as strong as the cloud albedo feedback. Against this background, the prevalence of a profound bias in the central equatorial Pacific in coupled GCMs is a surprise. We acknowledge that there is no lack of causes of initial cooling to the equatorial SST due to imperfections in the individual components. For example, the lack of phytoplankton in the model ocean could lead to an underestimate of the solar radiation absorbed by the ocean (Murtugudde et al. 2002). The lack of sufficient vertical resolution of the ocean model may also lead to an excessive cooling of the surface ocean (Stockdale et al. 1998). The

winds are not perfect in the atmospheric models and the errors may induce excessive equatorial upwelling upon coupling. The surface heating from the atmospheric model may also be too weak even with the observed SST (Sun et al. 2003). However, the effects of these initial errors in the individual model components on the equilibrium SST of the coupled model depend on the feedbacks (Kiehl 1998, Sun et al. 2003). Given the existence of a myriad of strong negative feedbacks, why SST in this region simulated by a coupled model, appears to be sensitive to flux errors in the model components? Could it be that the strength of one or more negative feedbacks in the model underestimated? Or alternatively, could it be that the strength of one or more positive feedbacks in the model is overestimated?

A preliminary attempt to answer these questions was made by Sun et al. (2003). By examining the response of radiative and dynamical fluxes to ENSO in the NCAR CCM3, they noted that the negative feedback of cloud albedo is substantially underestimated in the model. In further light of some coupled experiments, they put forward the hypothesis that a weaker regulating effect from the atmosphere may be a significant contributor to the development of an excessive cold-tongue in the corresponding coupled model. The purpose of this study is to extend the same analysis to eight additional models whose corresponding coupled runs also have an excessive cold-tongue in the equatorial Pacific. The almost ubiquitous presence of an excessive cold-tongue in the equatorial Pacific in the coupled GCMs offers a unique opportunity to understand the causes for this syndrome: a hypothesis developed in one model can be readily tested against other models.

2. Methods

The study employs the same method of Sun et al. (2003). We use the surface warming and cooling associated with ENSO as the forcing signal. We will then examine how radiative fluxes at the top of the atmosphere (TOA) and the vertically integrated transport of energy in the atmosphere vary in relation to the underlying SST. We quantify the feedbacks by linearly regressing the corresponding fluxes to the SST using their respective interannual variations.

The cloud and water vapor feedbacks in this paper are measured in the same way as that of Cess and Potter (1988): water vapor feedback is equated with the change in the greenhouse effect in the clear sky region, and the cloud feedbacks are equated with the corresponding changes in the long-wave and short-wave cloud forcing. These measures are not the same as the measures of Wetherald and Manabe (1988) which use offline radiative transfer calculations to obtain the true partial derivatives (Soden et al. 2004). The measures of Cess and Potter (1988) tend to overestimate the feedback from the greenhouse effect of water vapor and underestimate the feedback from the greenhouse effect of clouds. However, provided the feedbacks in the models are measured in the same way as in the observations, the errors revealed in the analysis are still true errors in the models. The available radiation data measure the feedbacks of water vapor and clouds on the ENSO time-scale in the form of Cess and Potter (1988). Also, the concern here is more with the combined effect of water vapor and cloud feedbacks on the response in the net surface heat flux into the ocean—the net atmospheric feedback—than with the accuracy in the definition of individual feedbacks of water vapor and clouds, the distinctions between the measures of Cess and Potter (1988) and Wetherald and Manabe (1988) of the individual feedbacks of water vapor and clouds are considered less important.

The observational data for radiation fluxes come from the Earth's Radiation Budget Experiment (ERBE) (Barkstrom et al. 1989). The data for the atmospheric transport is calculated from the National Center for Atmospheric Research (NCAR) and the National Center for Environmental Prediction (NCEP) reanalysis by making use of the global observations of temperature, humidity, and winds (Trenberth and Guillemot 1998). The data for the surface heat flux are obtained through the energy balance equation of the atmosphere—the surface heat flux is calculated by combining the net radiation flux from ERBE, the atmospheric transport, and the heat storage in the atmosphere (Trenberth et al. 2001). The data for the surface heat flux are considered the best available. Nonetheless, we will also calculate the feedback from the surface heat flux and the feedback from the atmospheric transport by making use of the ECMWF reanalysis (ERA-40) (Uppala et al. 2004). (The ERA-40 does not have data for the atmospheric transport. We will calculate it as the difference between the net surface heat flux and the net radiative flux at the top of the atmosphere from ERBE.)

The model data are from the runs of AMIP (Atmospheric Model Inter-comparison Project) over the ERBE period. The AMIP runs have the observed, time-varying SST as the boundary conditions. Therefore, the model atmosphere is subject to the same SST forcing as the real atmosphere.

The models that have been analyzed are the models that have a corresponding coupled run without the use of flux adjustment. These models are (1) the NCAR Community Climate Model Version 1 (CAM1) (Kiehl et al. 1998), (2) the NCAR Community Climate Model Version 2 (CAM2) (Collins et al. 2003), (3) the NCAR Community Climate Model Version 3 (CAM3) at

T42, (4) the NCAR CAM3 at T85 (Collins et al. 2004), (5) the NASA Seasonal-to-Interannual Prediction Project (NSIPP) model (Chou and Suarez 1996, Suarez 1995), (6) the Hadley Centre Model (Collins et al. 2001), (7) the French IPSL/LMDZ-4 (Hourdin et al. 2005), (8) the Geophysical Fluid Dynamics Laboratory (GFDL) AM2p10, and (9) the GFDL AM2p12 (The GFDL Global Atmospheric Model Development Team, 2004). (The GFDL AM2p10 is an earlier version of the GFDL AM2p12. The main differences between the two versions are in the use of boundary layer schemes and in the vertical layers. The AM2p10 uses the boundary layer scheme of Mellor and Yamada (1974) while the AM2p12 uses the boundary layer scheme of Lock et al. (2000). The AM2p12 has 24 vertical layers while the AM2p10 has 18 vertical layers).

The nine models involve the use of five different schemes for most convection. The NCAR models use the deep convection scheme by Zhang and McFarlane (1995) and the shallow convection scheme by Hack (1994). The NASA NSIPP model and the two GFDL models use the Relaxed Arakawa Schubert (RAS) scheme (Moorthi and Suarez 1992). The Hadley Centre model uses a mass-flux scheme (Gregory 1990, Gregory and Rowntree 1990) that is based on the bulk cloud model of Yanai et al. (1973). The French IPSL/LMDZ4 uses a revised version of the Emanuel (1991) scheme(Grandpeix et al., 2004). The nine models also have different vertical and horizontal resolutions. The vertical resolutions vary from 18 layers (NCAR CAM1) to 34 layers (NASA NSIPP). Except the NCAR CAM3 at T85, the horizontal resolutions of the models are more comparable--the horizontal resolutions in the remaining eight models vary from about 3.8^{o}X2.5^{o} in the Hadley Centre model to 2.5^{o}X2.0^{o} in the GFDL and the NASA models. Despite the many differences in these atmosphere models, gauged by the meridional and zonal SST gradients over the equatorial Pacific, all their corresponding coupled models have an excessive

cold-tongue over the central equatorial Pacific (Fig. 1).

3. Results

The estimates of the feedbacks from these models over the central equatorial Pacific region (150^{o}E-250^{o}E, 5^{o}S-5^{o}N) are summarized in Table 1. Note that these feedbacks are regional feedbacks on the ENSO time-scale. The results presented in the table are not sensitive to small changes in the boundaries chosen for the calculations. The definition of the symbols and the procedure of the calculations are the same as in Sun et al. (2003). $\frac{\partial}{\partial T}G_a$ is the water vapor feedback (the feedback from the clear-sky greenhouse effect including the effect of both water vapor and lapse rate), $\frac{\partial}{\partial T}C_l$ is the feedback from the long-wave forcing of clouds (the greenhouse effect of clouds), $\frac{\partial}{\partial T}C_s$ is the feedback from the short-wave forcing of clouds, and $\frac{\partial}{\partial T}D_a$ is the feedback from the atmospheric transport. $\frac{\partial F_a}{\partial T} = \frac{\partial G_a}{\partial T} + \frac{\partial C_l}{\partial T} + \frac{\partial C_s}{\partial T} + \frac{\partial D_a}{\partial T}$ and is termed the net atmospheric feedback. $\frac{\partial}{\partial T}F_s$ is the feedback from net surface heat flux into the ocean. Neglecting the heat storage in the atmosphere, which is small (Sun 2000), $\frac{\partial}{\partial T}F_s$ differs from $\frac{\partial}{\partial T}F_a$ by a constant—the rate of change of the ocean's surface emission with respect to SST. The numbers in parentheses are from the ERA-40 reanalysis. $\frac{\partial}{\partial T}F_s$ and $\frac{\partial}{\partial T}D_a$ estimated from the ERA-40 reanalysis are quite comparable to those from the NCAR-NCEP reanalysis.

With the exception of the two GFDL models and the French model, all models underestimate the negative feedback from the cloud albedo and the negative feedback from the atmospheric transport. The underestimate in the cloud albedo appears to be particularly worrisome as this feedback in one of these models has the opposite sign to the observed. The NCAR CAM2 differs

from the observed value in its simulation of the cloud albedo feedback by as much as 12.8 $W/m^2/K$. The NCAR CAM3 does not do much better. The NCAR CAM3 at T85 resolution, however, gets very close to the observed value. With the exception of the two GFDL models and the French model, the underestimate of the strength of the negative feedback from the atmospheric transport in these models are also significant. The error ranges from 2.4 $W/m^2/K$ in the CAM3 at T85 resolution to 7.7 $W/m^2/K$ in the NCAR CAM3 at the standard resolution.

All models have a stronger water vapor feedback than that indicated by ERBE observations. The differences between the modeled water vapor feedback and the feedback from the ERBE observations range from 15%--50%. The GFDL AM2p10 has the smallest discrepancy with the ERBE observations in the simulation of the water vapor feedback while the largest discrepancy is found in the Hadley Centre model. The differences between the water vapor feedback in the model simulations and that from ERBE observations could be in part due to the sampling differences between ERBE and the model data—the latter were obtained by the method of Cess and Potter (1988). Compared to the model data, ERBE under-samples the moist conditions (Zhang et al. 1994). Consequently ERBE observations may underestimate the changes of the greenhouse effect of water vapor from La Niña (cold and dry conditions) to El Niño (warm and moist conditions), and therefore underestimate the feedback of water vapor during ENSO. The bias due to the inadequate sampling does not explain the large range in the discrepancy between the water vapor feedback simulated by models and the water vapor feedback from ERBE observations. It may be prudent to continue to assume that at least on a regional scale and during ENSO, some models continue to have problems in simulating accurately the water vapor

feedback. Note that the water vapor feedback referred here includes the effect of water vapor as well as the lapse rate.

While it appears that some models may have significant errors in their simulations of water vapor feedback over the equatorial cold-tongue region, the results do not suggest that the corresponding feedbacks on a global scale also have significant errors. Indeed, since the work of Sun and Oort (1995) and Sun and Held (1996), there have been a number of studies looking at tropical or global mean changes in the greenhouse effect of water vapor (Soden 1997, Soden et al. 2002, Bauer et al. 2002, and Allan et al. 2003). These studies generally conclude that the response of the tropical mean greenhouse effect of water vapor to El Niño warming is fairly close to that from observations. Further studies are needed to reconcile the differences seen on a regional scale with the agreements on a global scale. For now, it is noted that the tropical averaged signal of Ga associated with ENSO is much weaker than the signal right over the equatorial cold-tongue region because of cancellations between different regions (Fig. 2).

Models also vary on the estimate of the feedback from the long-wave forcing of clouds, but they do not bias toward the same direction. While the NCAR CCM3 (CAM1) overestimates the feedback from the long-wave forcing of clouds by 3.7 $W/m^2/K$, the NCAR CAM2 underestimates this feedback by 5.6 $W/m^2/K$. The underestimate of the feedback from the long-wave forcing of clouds in the Hadley Centre model is also large (4.6 $W/m^2/K$). In four of the nine models--NCAR CAM2, NCAR CAM3, NASA/NSIPP, HadAM3, there is a significant compensation between the error in the estimate of the feedback from the long-wave forcing of clouds and the errors in the feedback from the greenhouse effect of water vapor—models

overestimate the water vapor feedback tends to underestimate the feedback from the long-wave forcing of clouds. In these four models, the total feedback from the greenhouse effect of water vapor and clouds is much closer to its observed counterpart than either individual component. This again suggests that the model—observation differences could be in part due to the differences between the sampling method of ERBE and that of model data.

The negative net atmospheric feedback in all models except the two GFDL models is underestimated over the region of concern. For most of these models, the underestimate of the strength of the net atmospheric feedback is because of the underestimate of the negative feedbacks from the cloud shortwave forcing and the atmospheric transport, and to a less degree because of the overestimate of the positive feedback from water vapor. For the French IPSL/LMDZ4, an overestimate of the positive feedbacks from the greenhouse effect of water vapor and clouds is the dominant cause for the underestimate of the net negative feedback from the atmosphere and hence the regulating effect from the atmosphere. The results confirm the suspicion that underestimating the regulatory effect from the atmosphere over the underlying SST in the region of concern is a prevalent problem in climate models. The results from the GFDL models (compared with other models), however, are very encouraging. The net atmospheric feedback in the two GFDL models is comparable to the observed value. The improvements in the GFDL models (relative to CAM2/3) are not just from the improvements in the cloud albedo feedback, but also from the improvements in the feedback from the atmospheric transport.

The horizontal pattern of the response in G_a to ENSO forcing from the models show remarkable agreement with each other and with observations (Fig. 2). The corresponding response of C_l has more variability (Fig. 3). The NASA model is particularly notable--the response of C_l in the equatorial central Pacific near the dateline (180^oE-140^oW) is much weaker than the observed (Fig. 3f). This equatorial minimum response splits the response of C_l to El Niño warming into two parts, each of which has a maximum off the equator. Such a split still exists when the response of G_a and the response of C_l are added together (Fig. 4f). It is again interesting to note, however, that the response in the total greenhouse effect ($G_a + C_l$) in many models appears to have a better agreement with that in the observations than the response of C_l alone (Fig.4). Clearly, an overestimate of the total greenhouse effect is not a problem of all models.

The response of C_s and the rainfall in the NASA model also has the same "split pea" feature (compare Fig.5f with Fig.6f), indicating a lack of response of convection in the central equatorial Pacific near the date line in the model. The lack of response of D_a in the same region in the NASA model (Fig. 7f) also suggests a lack of response of convection in the central equatorial Pacific.

Contrasting the spatial patterns in the response of the cloud forcing (Fig.3 and Fig.5) with the spatial patterns in the rainfall (Fig.6) confirms the impression that the leading source of errors in the response of C_s may still be the most obvious: errors in the response of convection. The rainfall responses in the equatorial central Pacific in the CAM2 and CAM3 are the two weakest, so are their responses in C_s. The rainfall response in the CAM3 at T85 resolution is improved relative to the standard CAM3, so is the response of C_s. The improvement in the response in C_s

in the HadAM3 and the GFDL models (compared with CAM2 and CAM3) apparently also follow the improvement in the response of convection. All models predict a maximum precipitation response over the equator east of the dateline, but the GFDL models have the strongest responses in this region.

The response of convection in the model does not have the same control over the response of C_l as over the response of C_s: the HadAM3 has a response in rainfall that is comparable to observations, but the response in C_l in the same model is only half of the value from observations. Convection also has a lesser control over the response in G_a. For example, the rainfall in the NCAR CAM2 and CAM3 is much weaker than that in CAM1, but the response in G_a in the NCAR CAM2 and CAM3 is only slightly weaker than that in CAM1.

The two GFDL models and the French model simulate well the spatial pattern of the response in D_a, but all other models do not (Fig. 7). The cause of their poor simulation of the response of D_a is apparently the same as the cause of their relatively poor simulation of the response of C_s: the lack of response of convection on the equator near the date line region. The response in precipitation over the central equatorial Pacific in the NCAR models is not distinctly weak though there is a distinct lack of response in D_a in that region. However, the responses in the precipitation in the NCAR CAM2 and the NCAR CAM3, are weak throughout the concerned region (Fig. 6c, d).

The impact of the errors in the aforementioned feedbacks on the response of the net surface heating (F_s) is further shown in Fig. 8, which gives a basin-wide, and a more critical view of the

response of the model atmosphere. In five of the nine models (the NCAR CAM1, CAM2, CAM3 at T42 resolution, CAM3 at T85 resolution, and the NASA model, the response of the surface heating to El Niño warming in the equatorial central Pacific (160^{o}E-140^{o}W) has the wrong sign. The response of F_s in the Hadley Centre model in the same region is near zero. The response of F_s in the French model has the correct sign in the region of concern, but weaker in magnitude. The two GFDL models have adequate responses in the equatorial central Pacific. One of them—the GFDL AM2p10-- suffers a significant deficiency in the region east to about 120^{o}W. The negative response in the GFDL AM2p10 also does not extend as far west as in the observations. The zonal extent of the response in the later version of the GFDL model—the AM2p12—is improved, but the meridional extent of the response is more confined. Nonetheless, the spatial pattern of the response of F_s in both the GFDL models resembles the observed remarkably well.

Diagnosing the root causes of all the model deficiencies is beyond the scope of the present paper and would require more sophisticated tools than simple regression analysis here. The encouraging part of the present analysis is that it is possible to for the model atmosphere to have a regulating effect that is comparable in strength to the real atmosphere: the GFDL AM2p10 provides an example. Whether this good agreement between the simulations by the GFDL model and the observations is simply a matter of luck or truly reflecting the fidelity of the model to nature needs to be further examined. For now, we note that the precipitation response over the equator in the GFDL models is stronger than in the observations. In fact, normalized the maximum precipitation response over the equator, the two GFDL models still underestimate the strength of the negative feedback from cloud albedo. The feedback from the total greenhouse

effect in the GFDL AM2p12 also appears to be too strong to be explained by the possible errors in the ERBE observations.

4. Discussion

These results confirm the suspicion that an underestimate of the regulatory effect from the atmosphere over the equatorial Pacific region is a prevalent problem. Most models underestimate the strength of the negative feedback from cloud albedo and the strength of the negative feedback from atmospheric transport. The underestimate of the strength of these negative feedbacks is linked to an underestimate of the response of precipitation over the equator. All models have a stronger water vapor feedback than that indicated in ERBE observations. The degree of the overestimate of the water vapor feedback varies considerably among the models.

While the analysis has revealed some common deficiencies in the simulation of atmospheric feedbacks by GCMs, the results also suggest that the common errors in the atmospheric feedbacks are unlikely the sole cause of the excessive cold-tongue in the central equatorial Pacific. The simulation of the strength of the net atmospheric feedback in the GFDL AM2p10 is probably as close to the observed as one can reasonably hope, but the corresponding coupled model still has an excessive cold-tongue (Fig. 1i). The results highlight the need to look at the ocean feedbacks. One way to do so is to check the response of the surface wind stress to changes in the SST and then the response of the ocean heat transport to the changes in the wind stress. The former can be assessed to some degree using the AMIP runs of the atmospheric GCMs. The obstacle for carrying out this analysis immediately is the lack of good data for the tropical wind stress. The limited satellite data (Liu 2002) has revealed severe deficiencies in the NCEP

reanalysis, but the satellite data are still too short for calculating feedbacks. The latter requires forced ocean experiments from different groups using the same surface forcing. These forced ocean model experiments are not yet available on the scale of the AMIP experiments. Nor is it clear whether the accuracy of ocean heat transport data is sufficient to validate the results from the model experiments.

The present analysis has a linear perspective built in, and therefore the results are more relevant for the initial development of the excessive cold-tongue. After a significant cold SST bias in the central equatorial Pacific develops in the modeled climate, it may displace the convection so far west that the associated atmospheric feedbacks cease operating in the central equatorial Pacific. The study by Wittenberg et al. (2004) suggests that GFDL models may have this nonlinear effect. Other models probably have this nonlinear effect too. Nonetheless, it is logical to first identify the factors that are responsible for the initial growth of the excessive cold-tongue and then examine how excessive cold-tongue in the coupled model maintains its stability. This consideration of priorities points a direction to extend the present study, which is to directly use the outputs from coupled models to quantify the feedbacks in the cold-tongue region. The drawback of using the ENSO signals in the coupled models is that the signals are not the same as in the real world, but the results may shed light on the question of how the excessive cold-tongue in the coupled model maintains its stability.

Underestimating the negative feedbacks in the central equatorial Pacific does not suggest that the models overestimate global warming. What have assessed here are regional feedbacks on the time-scale of ENSO. The forcing due to increases in CO_2 is not the same as the El Niño

warming. While bearing this difference in mind, one also notes that many coupled GCMs do predict El Niño-like warming in response to increases in CO_2 (Meehl and Washington 1996, Timmerman et al. 1999, Cai and Whetton 2000, Boer et al. 2004). Therefore, the feedbacks inferred from the response to El Niño warming may not be entirely irrelevant to the feedbacks in global warming. In any case, our confidence with the model predictions of global warming may have to come from how well the models simulate the feedbacks on the shorter time-scales because it is over these time-scales we have better data and know more quantitatively the feedbacks in nature.

References:

Allan, R.P., M.A. Ringer, and A. Slingo, 2003: Evaluation of moisture in the Hadley Centre climate model using simulations of HIRS water-vapor channel radiances. Q.J.R. Meteorol. Soc., **129**, 3371-3389.

Barkstrom, B.R., E.F. Harrison, G.L. Smith, R. Green, J. Kibler, R.D. Cess, and the ERBE Science Team, 1989: Earth Radiation Budget Experiment (ERBE) Archive and April 1985 Results. *Bull. Amer. Meteror. Soc.,* **70**, 1254-1262.

Bauer, M., A.D. Del Gienio, J.R. Lanzante, 2002: Observed and simulated temperature-humidity relationships: sensitivity to sampling and analysis. *J. Climate,* 15, 203-215.

Boer, G.J., B. Yu, S.-J. Kim, and G.M. Flato, 2004: Is there observational support for an El Niño-like pattern of future global warming. *Geophys. Res. Lett.,* **31,** doi:10.1029/2003.

Boville, B. A., and P. R. Gent, 1998: The NCAR Climate System Model, Version One. *J. Climate,* 11, 1115-1130.

Cai, W., and P.H. Whetton, 2000: Evidence for a time-varying pattern of greenhouse warming in the Pacific Ocean, *Geophys. Res. Lett.,* **27**, 2577-2580.

Cess, R. D., and G. L. Potter, 1988: A methodology for understanding and intercomparing atmospheric climate feedback processes in general circulation models. J. Geophys. Res., 93, 8305–8314.

Chou, M.-D., and M.J. Suarez, 1996: A Solar Radiation Parameterization (CLIRAD-SW). NASA Technical Memorandum no. 104606, v. 15, 48 pp.

Collins, W. D., J. J. Hack, B. A. Boville, P. J. Rasch, D. L. Williamson, J. T. Kiehl, B. Briegleb, J. R. McCaa, C. Bitz, S.-J. Lin, R. B. Rood, M. Zhang, and Y. Dai, 2003: Description of the

NCAR Community Atmosphere Model (CAM2). 171pp. [Available online at http://www.ccsm.ucar.edu/models/atm-cam/docs/cam2.0/description.pdf.]

Collins, W. D., P. J. Rasch, B. A. Boville, J. J. Hack, J. R. McCaa, D. L. Williamson, J. T. Kiehl, B. Briegleb, C. Bitz, S.-J. Lin, M. Zhang, and Y. Dai, 2004: Description of the NCAR Community Atmosphere Model (CAM 3.0), Technical Report NCAR/TN-464+STR, National Center for Atmospheric Research, Boulder, Colorado, 210 pp.

Collins, M., S.F.B. Tett, and C. Cooper, 2001: The internal climate variability of a HadCM3, a version of the Hadley Centre coupled model without flux adjustments. *Clim. Dyn.,* 17: 61-81.

Delworth, T. L., et al., 2004: GFDL's CM2 global coupled climate models - Part I: Formulation and simulation characteristics. J. Climate (submitted)

Emanuel, K. A., 1991: A scheme for representing cumulus convection in large-scale models, J. Atmos. Sci., **48**, 2313-2335.

Fu, R., DelGenio, A.D., Rossow, W.B., and Liu, W.T., 1990: Cirrus cloud thermostat for tropical sea surface temperature tested using satellite data. *Nature*, 358, 394-397.

Grandpeix, J.-Y., V. Phillips, and R. Tailleux, 2004: Improved mixing representation in Emanuel's convection scheme, Q. J. R. Meteorol. Soc. 130, 3207-3222.

Gregory, D., 1990: Convection scheme. Unified Model Documentation Paper No. 27, United Kingdom Meteorological Office, Bracknell, Berkshire RG122SZ, UK.

Gregory, D., and P.R.R. Rowntree, 1990: A mass flux convection scheme with representation of cloud ensemble characteristics and stability dependent closure. Mon. Wea. Rev., 118, 1483-1506.

Hack, J. J., 1994: Parameterization of moist convection in the National Center for Atmospheric Research Community Climate Model (CCM2). *J. Geophys. Res.,* **99**, 5551-5568.

Hourdin, F., I. Musat, S. Bony, P. Braconnot, F. Codron, J.-L. Dufresne, L. Fairhead, M.-A. Filiberti, P. Friedlingstein, J.-Y. Grandpeix, G. Krinner, P. LeVan, Z.-X. Li, F. Lott, 2005 The LMDZ4 general circulation model: climate performance and sensitivity to parametrized physics with emphasis on tropical convection. *Climate Dynamics*, submitted.

Kiehl, J.T., 1998: Simulation of the tropical Pacific warm-pool with the NCAR climate system model. *J. Climate,* **11**, 1342-1355.

Kiehl, J., J. J. Hack, G. Bonan, B. A. Boville, D. Williamson, and P. J. Rasch, 1998: The National Center for Atmospheric Research Community Climate Model: CCM3. *J. Climate*, 11, 1131-1149.

Kiehl, J. T., and P. R. Gent, 2004: The Community Climate System Model, Version Two. J. Clim., 17, 3666-3682.

Liu, W. T., 2002: Progress in scatterometer applications. *J. Oceanogr*., 58, 121–136.

Lock, A. P., A. R. Brown, M. R. Bush, G. M. Martin, and R. N. B. Smith, 2000: A new boundary layer mixing scheme. Part I: Scheme description and single-column model tests. Mon. Wea. Rev., 128, 3187-3199.

Marti O., P. Braconnot, J. Bellier, R. Benshila,S. Bony, P. Brockmann, P. Cadulle, A. Caubel, S. Denvil, J.L. Dufresne, L. Fairhead, M.-A. Filiberti,T. Fichefet, P. Friedlingstein, J.-Y. Grandpeix, F. Hourdin, G. Krinner, C. Levy, I. Musat, and C. Talandier, 2005: The new IPSL climate system model: IPSL CM4(available at http://dods.ipsl.jussieu.fr/omamce/IPSLCM4/DocIPSLCM4/FILES/DocIPSLCM4.pdf)

Meehl, G.A., and W. M. Washington, 1996: El Niño-like climate change in a model with increased atmospheric CO2 concentrations. *Nature,* **382**, 56-60.

Mellor, G.L., and T. Yamada, 1974: A hierarchy of turbulence closure models for planetary

boundary layers, *J. Atmos. Sci.* ,**31**, 1791-1806.

Moorthi, S. and M. Suarez, 1992: Relaxed Arakawa-Schubert: a parameterization of moist convection for general circulation models. Mon. Wea. Rev., 120, 978-1002.

Murtugudde, R., J. Beauchamp, C. R. McClain, and A. J. Busalacchi, 2002: Effects of penetrative radiation on the upper tropical ocean circulation. *J. Climate*, 15, 470-496.

Press, W.H., S.A. Teukolsky, W.T. Vetterling, and B.P. Flannery, 1992, Numerical Recipes, Cambridge University Press, 963 pp.

Pierrehumbert, R. T., 1995: Thermostats, radiator Fins, and the local runaway greenhouse. *J. Atmos. Sci.,* 52, 1784-1806.

Ramanathan, V. and W. Collins, 1991: Thermodynamic regulation of ocean warming by cirrus clouds deduced from observations of the 1987 El Niño. *Nature*, 351, 27-32.

Rayner, N. A., Horton E. B., Parker D. E., Folland C. K., and Hackett R. B., 1996: Version 2.2 of the global sea-ice and sea surface temperature data set, 19031994. Climate Research Tech. Note 74 (CRTN74), Hadley Centre for Climate Prediction and Research, Met Office, United Kingdom, 35 pp.

Soden, B.J., 1997: Variations in the tropical Greenhouse effect during El Niño. *J. Climate*, **10**, 1050-1054.

Soden, B., A.J. Broccoli, and R.S. Hemler, 2004: On the Use of Cloud Forcing to Estimate Cloud Feedbacks. *J. Climate*, **17**, 3661—3665.

Soden, B.J., R.T. Wetherald, G.L. Stenchikov, A. Robock, 2002: Global Cooling After the Eruption of Mount Pinatubo: A Test of Climate Feedback by Water Vapor. *Science,* **296,** 727—730.

Stockdale, T.N., A.J. Busalacchi, D.E. Harrison, and Richard Seager, 1998: Ocean Modeling for

ENSO. *J. Geophys. Res.,* 103, 14,325-14,355.

Suarez, M.J., 1995: Documentation of the ARIES/GEOS Dynamical Core, version 2. NASA Technical Memorandum no. 104606, v. 5, 53 pp

Sun, D.-Z., 2000: The heat sinks and sources of the 1986-87 El Niño. *J. Climate*, **13**, 3533-3550.

Sun, D.-Z., and I. Held, 1996: A comparison of modeled and observed relationships between interannual variations of water vapor and temperature. *J. Climate*, **9**, 665-675.

Sun, D.-Z. and Z. Liu, 1996: Dynamic ocean-atmosphere coupling: a thermostat for the tropics. *Science,* 272, 1148-1150.

Sun, D.-Z., J. Fasullo, T. Zhang, and A. Roubicek, 2003: On the radiative and dynamical feedbacks over the equatorial Pacific cold-tongue. *J. Climate.*, **16,** 2425—2432.

Sun, D.Z. and A.H. Oort, 1995: Humidity-temperature relationships in the tropical troposphere. *J. Climate*, **8**, 1974-1987.

Sun. D.-Z. and K. E. Trenberth, 1998: Coordinated heat removal from the tropical Pacific region during the 1986-87 El Niño. *Geophys. Res. Lett.,* 25, 2659-2662.

The GFDL Global Atmospheric Model Development Team, 2004: The new GFDL global atmosphere and land model AM2/LM2: Evaluation with prescribed SST simulations. *J. Climate*, **17,** 4641-4673.

Timmerman, A. J., J. Oberhuber, A. Bacher, M. Esch, M. Latif, and E. Roeckner, 1999: Increased El Niño frequency in a climate model forced by future global warming. *Nature,* **398,** 694-696.

Trenberth, K.E., and C.J. Guillemot, 1998: Evaluation of the atmospheric moisture and hydrological cycle in the NCEP reanalyses. *Climate Dyn.,* **14**, 213-231.

Trenberth, K.E., J.M. Caron, and D.P. Stepaniak, 2001: The atmospheric energy budget and

implications for surface fluxes and ocean heat transport. *Climate Dyn*., **17**, 259-296.

Uppala S., P. Kallberg, A. Hemandez, S. Saarinen, M. Florino, X. Li, K. Onogi, N. Sokka, U. Andrae, V. Da Costa, 2004: ERA-40: ECMWF 45 year reanalysis of the global atmosphere and surface conditions 1957-2002. ECMWF Newsletter No. 101—Summer/Autumn 2004:2-21.

Wallace, J.M., 1992: Effect of deep convection on the regulation of tropical sea surface temperature. *Nature*, 357, 230-231

Wetherald, R. T., and S. Manabe, 1988: Cloud feedback processes in a general circulation model. J. Atmos. Sci., 45, 1397–1415.

Wittenberg, A.T., A. Rosati, N.-C. Lau, and J. J. Ploshay, 2004: GFDL's CM2 Global Coupled Models, Part 3: Tropical Pacific Climate and ENSO. *J. Climate,* Submitted.

Xie, P., and P.A. Arkin, 1996: Analyses of Global Monthly Precipitation Using Gauge Observations, Satellite Estimates, and Numerical Model Predictions. *J. Climate,* **9**, 840-858.

Yanai, M., S. Esbensen, and J.-H., Chu, 1973: Determination of bulk properties of tropical cloud clusters from large-scale heat and moisture budgets. J. Atmos. Sci., 30, 611-627.

Zhang, G.J., and N. A. McFarlane, 1995: Sensitivity of climate simulations to the parameterization of cumulus convection in the Canadian Climate Centre general circulation model. *Atmos.-Ocean***, 33**, 407-446.

Zhang, M.H., R.D. Cess, T.Y. Kwon, and M.H. Chen, 1994: Approaches of comparison for clear-sky radiative fluxes from general circulation models with Earth Radiation Budget Experiment data. *J. Geophys. Res.,* **99**, 5515-5523.

Acknowledgments

This research was supported partially by NOAA's office of global programs (the Climate Dynamics Program and Experimental Prediction Program, and the CLIVAR Pacific Program), and partially by the NSF Climate Dynamics Program (ATM-9912434 and ATM-0331760). Using data from the Atmospheric Model Inter-comparison Project (AMIP), this work was also partially supported under the auspices of the U.S. Dept. of Energy, Office of Science, at the University of California Lawrence Livermore National Laboratory under Contract W-7405-Eng-48. The National Center for Atmospheric Research (NCAR) is sponsored by the National Science Foundation. The leading author (D.-Z. Sun) would like to thank Dr. Robert Dickinson for his encouraging comments. D.-Z. Sun would also like to thank Dr. Ping Chang and Dr. R. Saravanan for the conversations on the causes of the double ITCZ in coupled models. The helpful suggestions from the two anonymous reviewers and the editor Dr. Anthony Del Genio are also gratefully acknowledged.

Table Legends

Table 1: Atmospheric feedbacks over the equatorial Pacific (5^{o}S-5^{o}N, 150^{o}E-250^{o}E) from nine climate models. See text for the definition of the symbols for the various feedbacks. The values for these feedbacks are obtained through a linear regression using the interannual variations of the SST and the corresponding fluxes over the equatorial Pacific. The error bars are obtained using the method of Press et al. (1992) for the case in which the measurement errors of individual data points are not known. The numbers in parentheses are estimates from the ERA-40 reanalysis (the atmospheric transport Da is calculated as the difference between the net surface heat flux from the ERA-40 reanalysis and the net radiative flux at the top of the atmosphere from ERBE).

Figure Legends

Figure 1: Tropical Pacific SST from observations (Rayner et al. 1996) and nine coupled climate models: NCAR CCSM1 (Boville and Gent 1998), the NCAR CCSM2 (Kiehl and Gent 2004), the NCAR CCSM3 (www.ccsm.ucar.edu/experiments/ccsm3.0/), the NASA CGCM ((http://nsipp.gsfc.nasa.gov/data_req/coupled/coupl_data_main.htl), the coupled model of the Hadley Centre (HadCM3)(Collins et al. 2001), the French IPSL climate system model (IPSL-CM4) (Marti et al. 2005), and the two latest versions of the coupled models from GFDL (Delworth et al. 2004, http://data1.gfdl.noaa.gov/nomads/forms/decen/CM2.X/). The atmospheric components of the nine coupled models are respectively the NCAR CAM1, the NCAR CAM2, the NCAR CAM3 at the standard T42 resolution, the NCAR CAM3 at T85 resolution, the NASA NSIPP GCM, the Hadely Centre model HadAM3, the French IPSL/LMDZ4, the GFDL AM2p10, and the GFDL AM2p12. Shown are annual mean conditions.

Figure 2: Response of the greenhoue effect of water vapor (G_a) to El Niño warming. Shown are coefficents obtained by linearly regressing the greenhouse effect of water vapor at each grid point on the SST averaged over the equatorial Pacific (5^oS-5^oN, 150^oE-250^oE). The interannual variations of G_a over the ERBE period are used for the calculations.

Figure 3: Response of the greenhouse effect of clouds (C_l) to El Niño warming. Shown are coefficents obtained by linearly regressing the greenhouse effect of clouds at each grid point on the SST averaged over the equatorial Pacific (5^oS-5^oN, 150^oE-250^oE). The

interannual variations of the concerned quantities over the ERBE period are used for the calculations.

Figure 4: Response of the combined greenhouse effect of clouds and water vapor ($G_a + C_l$) to El Niño warming. Shown are coefficents obtained by linearly regressing the greenhouse effect of clouds and water vapor at each grid point on the SST averaged over the equatorial Pacific (5^oS-5^oN, 150^oE-250^oE). The interannual variations of the concerned quantities over the ERBE period are used for the calculations.

Figure 5: Response of the shortwave forcing of clouds (C_s) to El Niño warming. Shown are coefficents obtained by linearly regressing the short-wave forcing of clouds at each grid point on the SST averaged over the equatorial Pacific (5^oS-5^oN, 150^oE-250^oE). The interannual variations of the concerned quantities over the ERBE period are used for the calculations.

Figure 6: Response of the precipitation to El Niño warming. Shown are coefficents obtained by linearly regressing the precipitation at each grid point on the SST averaged over the equatorial Pacific (5^oS-5^oN, 150^oE-250^oE). The interannual variations of the concerned quantities over the ERBE period are used for the calculations. The precipitation data are from Xie and Arkin (1996).

Figure 7: Response of the convergence of vertically integrated transport of energy by the atmospheric circulations (D_a) to El Niño warming. Shown are coefficents obtained by linearly regressing the value of D_a at each grid point on the SST averaged over the

equatorial Pacific (5^oS-5^oN, 150^oE-250^oE). The interannual variations of the concerned quantities over the ERBE period are used for the calculations.

Figure 8: Response of the net surface heating (F_s) to El Niño warming. Shown are coefficents obtained by linearly regressing the net surface heating at each grid point on the SST averaged over the equatorial Pacific (5^oS-5^oN, 150^oE-250^oE). The interannual variations of the concerned quantities over the ERBE period are used for the calculations. The data used for Fs are the same as in Sun et al. (2003).

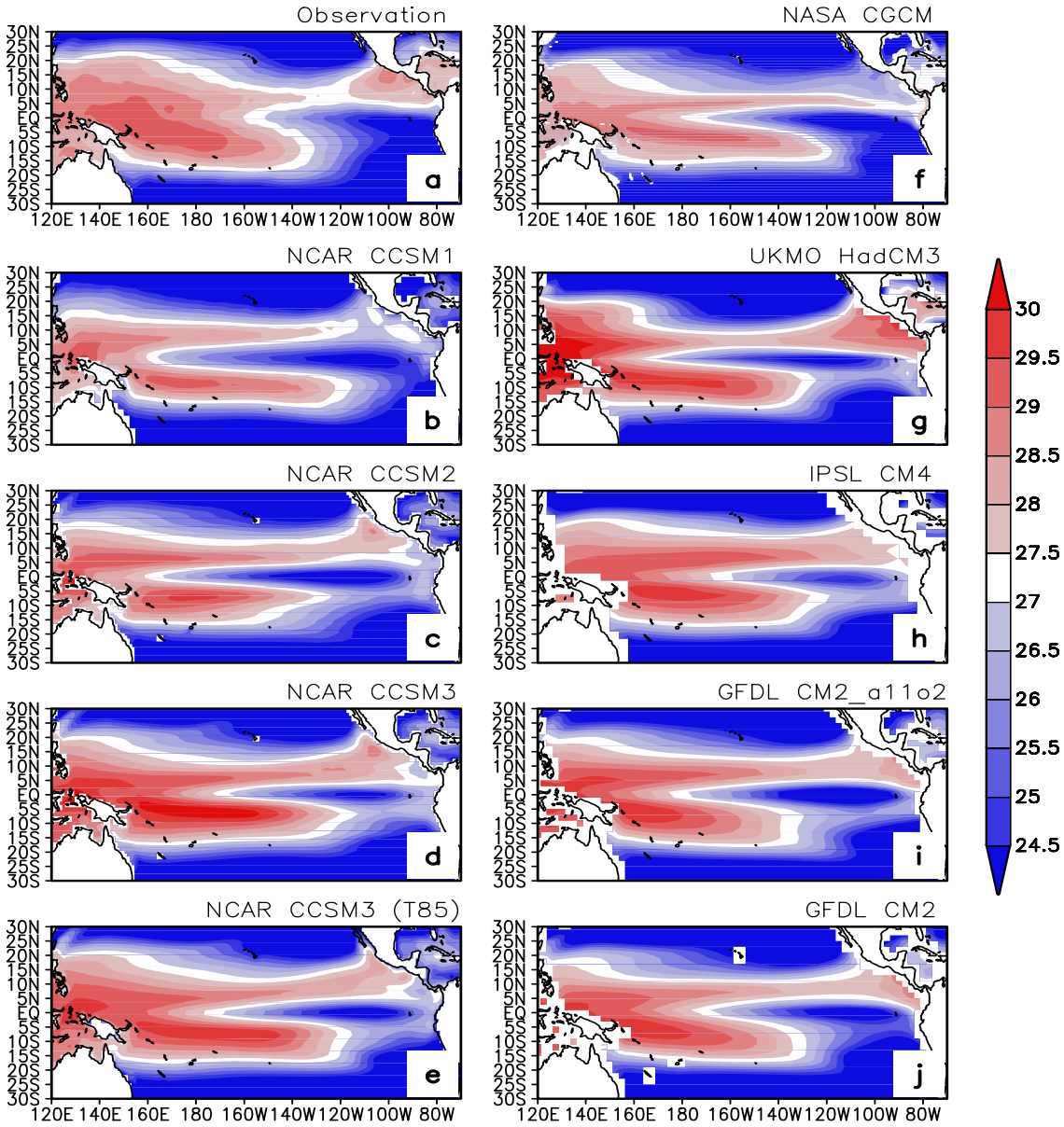

Figure 1: Tropical Pacific SST from observations (Rayner et al. 1996) and nine coupled climate models: NCAR CCSM1 (Boville and Gent 1998), the NCAR CCSM2 (Kiehl and Gent 2004), the NCAR CCSM3 (www.ccsm.ucar.edu/experiments/ccsm3.0/), t h e N A S A CGCM (http:// nsipp.gsfc.nasa.gov/data_req/coupled/coupl_data_main.htl), the coupled model of the Hadley Centre (HadCM3) (Collins e t a l . 2 0 0 1), the French IPSL climate system model (IPSL-CM4) (Marti et al. 2005), and the two latest versions of the coupled models from GFDL (Delworth et al. 2004, http://data1.gfdl.noaa.gov/nomads/forms/decen/CM2.X/). The atmospheric components of the nine coupled models are respectively the NCAR CAM1, the NCAR CAM2, the NCAR CAM3 at the standard T42 resolution, the NCAR CAM3 at T85 resolution, the NASA NSIPP GCM, the Hadely Centre model HadAM3, the French IPSL LMDZ4, the GFDL AM2p10, and the GFDL AM2p12. Shown are annual mean conditions.

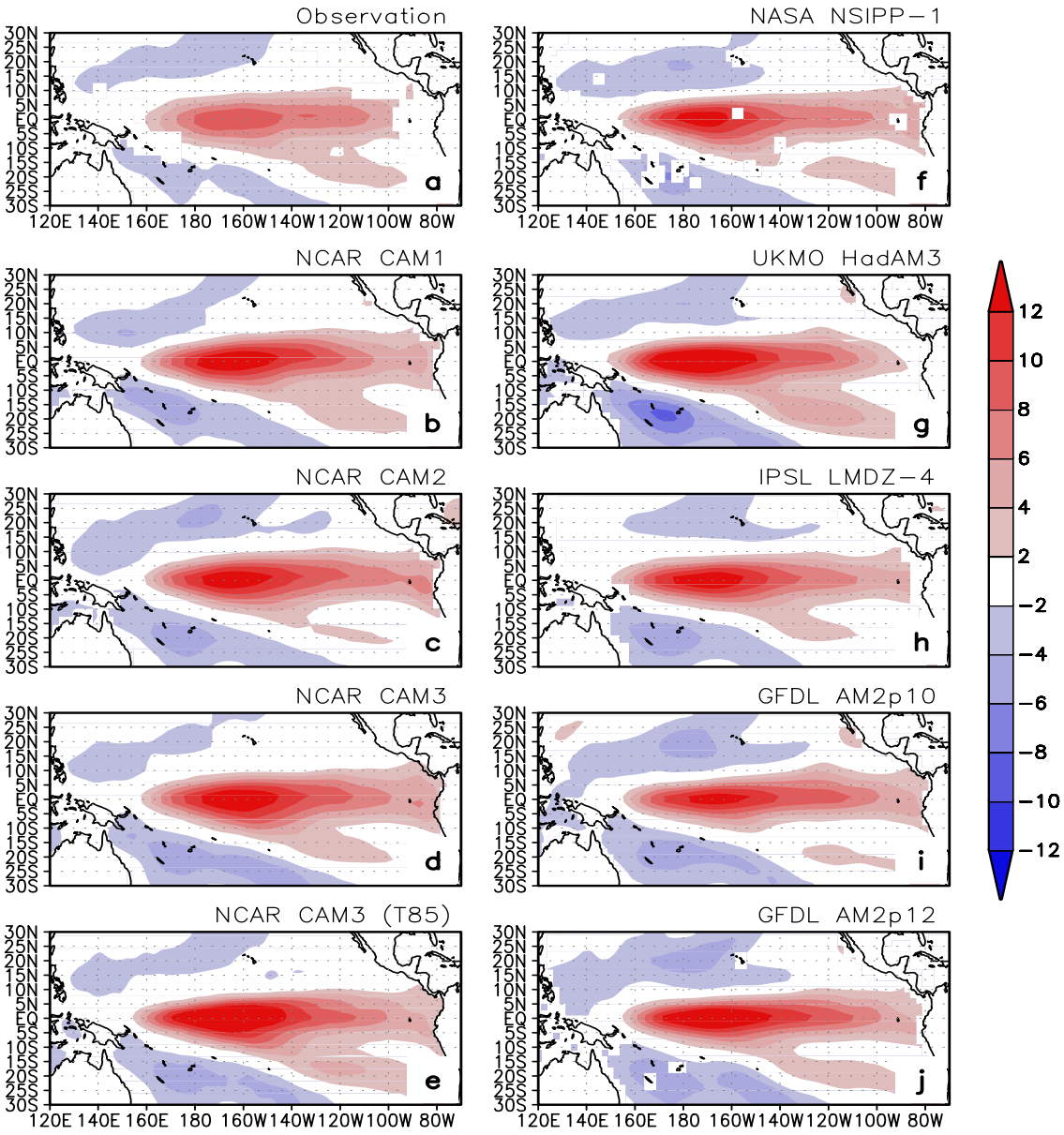

Figure 2: Response of the greenhoue effect of water vapor (Ga) to El Niño warming. Shown are coefficents obtained by linearly regressing the greenhouse effect of water vapor at each grid point on the SST averaged over the equatorial Pacific (5^{O}S-5^{O}N, 150^{O}-250^{O}E). The inter-annual variations of Ga over the ERBE period are used for the calculations.

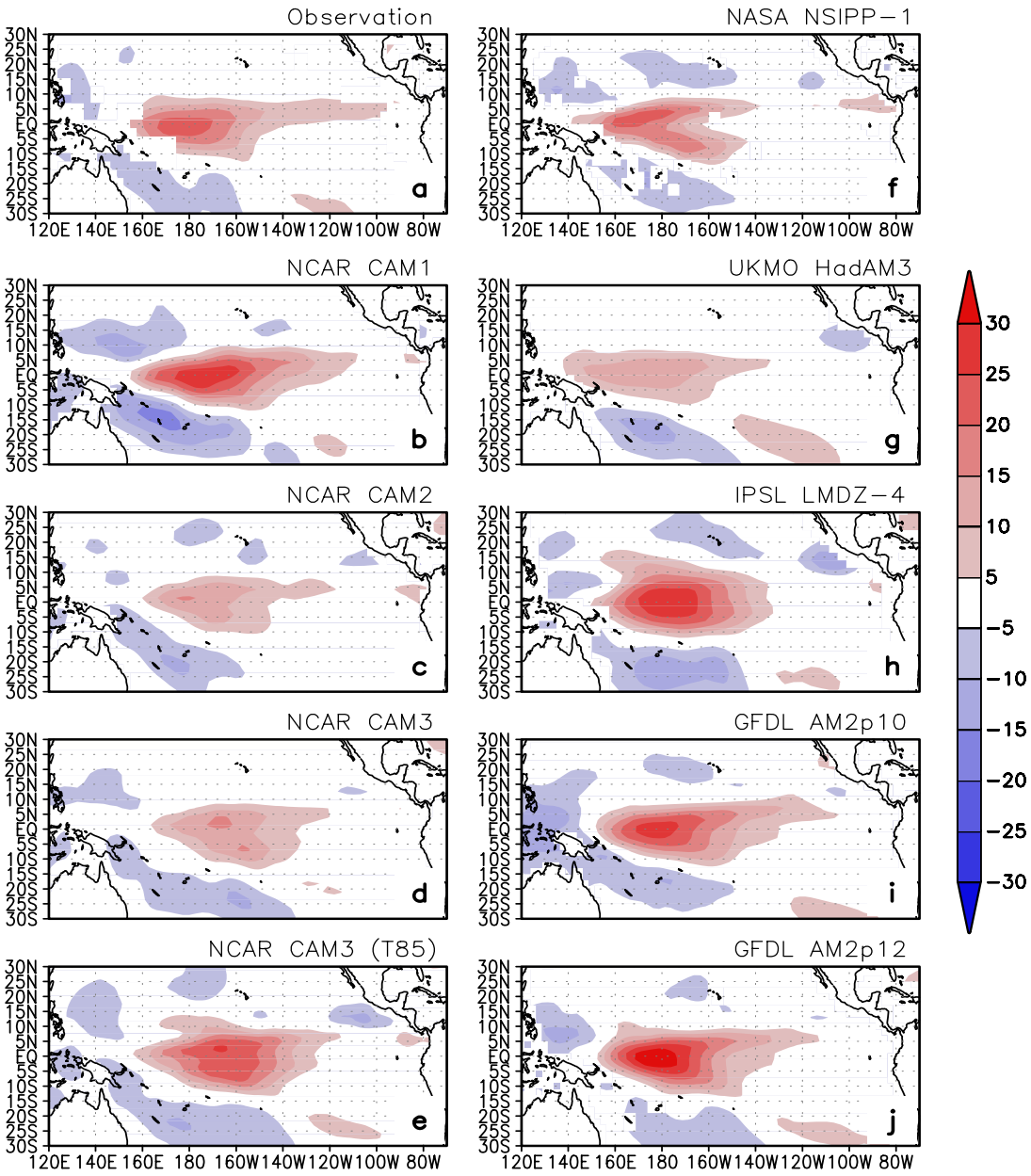

Figure 3: Response of the greenhouse effect of clouds (Cl) to El Niño warming. Shown are coefficents obtained by linearly regressing the greenhouse effect of clouds at each grid point on the SST averaged over the equatorial Pacific (5^{O}S-5^{O}N, 150^{O}E-250^{O}E). The interannual variations of the concerned quantities over the ERBE period are used for the calculations.

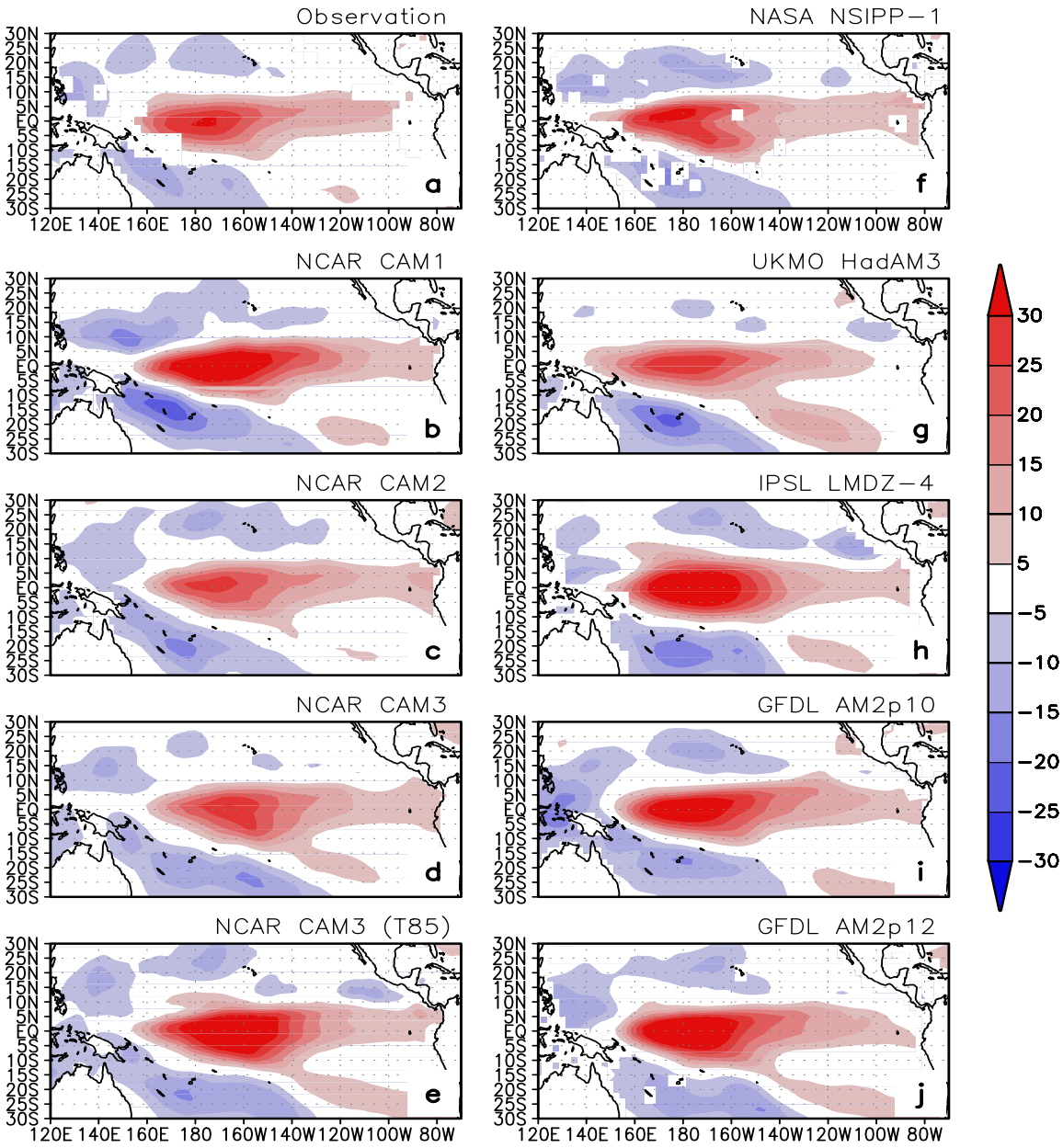

Figure 4: Response of the combined greenhouse effect of clouds and water vapor (Ga +Cl) to El Niño warming. Shown are coefficents obtained by linearly regressing the greenhouse effect of clouds and water vapor at each grid point on the SST averaged over the equatorial Pacific (5^{O}S-5^{O}N, 150^{O}E-250^{O}E). The interannual variations of the concerned quantities over the ERBE period are used for the calculations.

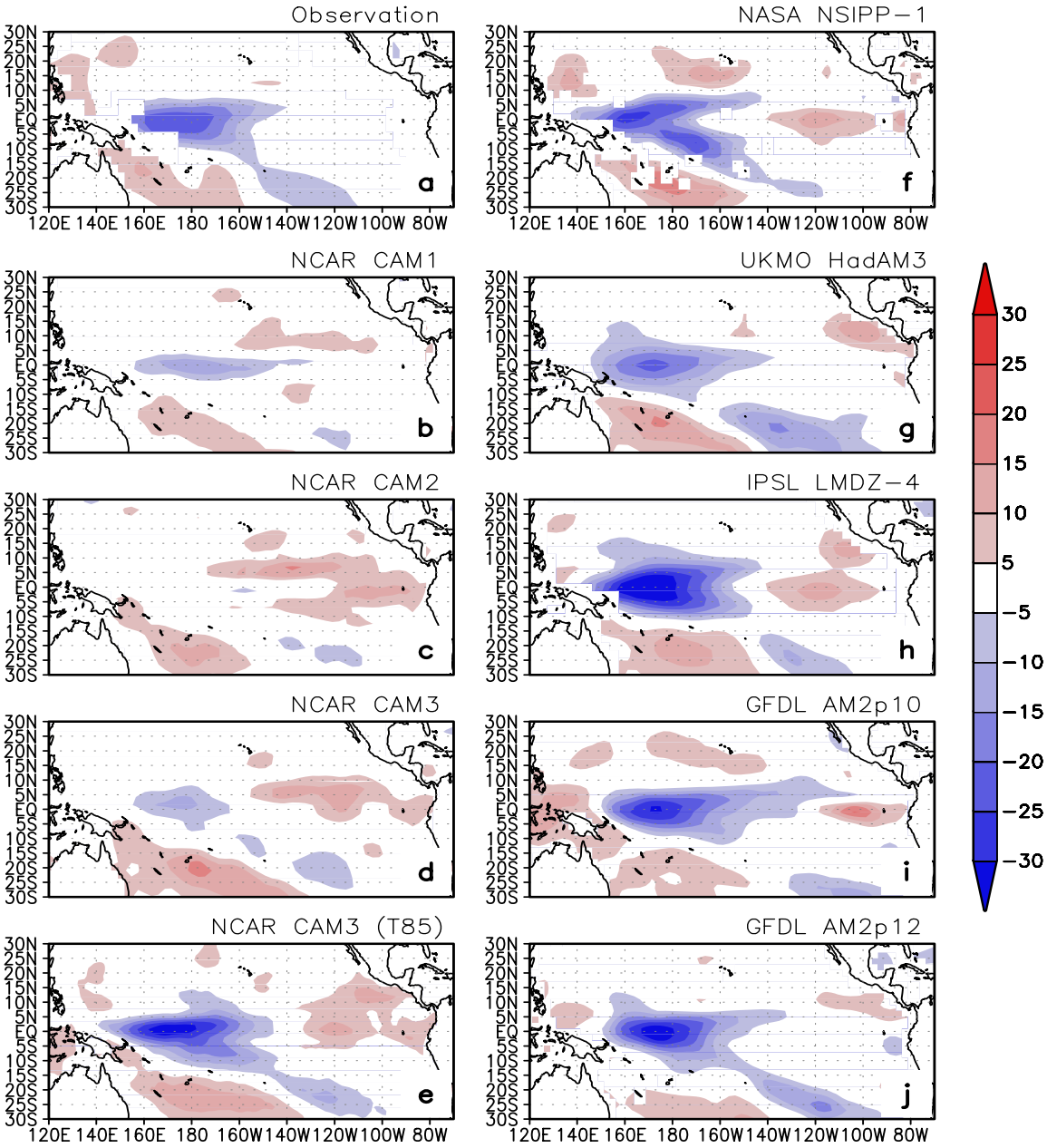

Figure 5: Response of the shortwave forcing of clouds (Cs) to El Niño warming. Shown are coefficents obtained by linearly regressing the short-wave forcing of clouds at each grid point on the SST averaged over the equatorial Pacific (5^{O}S-5^{O}N, 150^{O}-250^{O}E). The interannual variations of the concerned quantities over the ERBE period are used for the calculations.

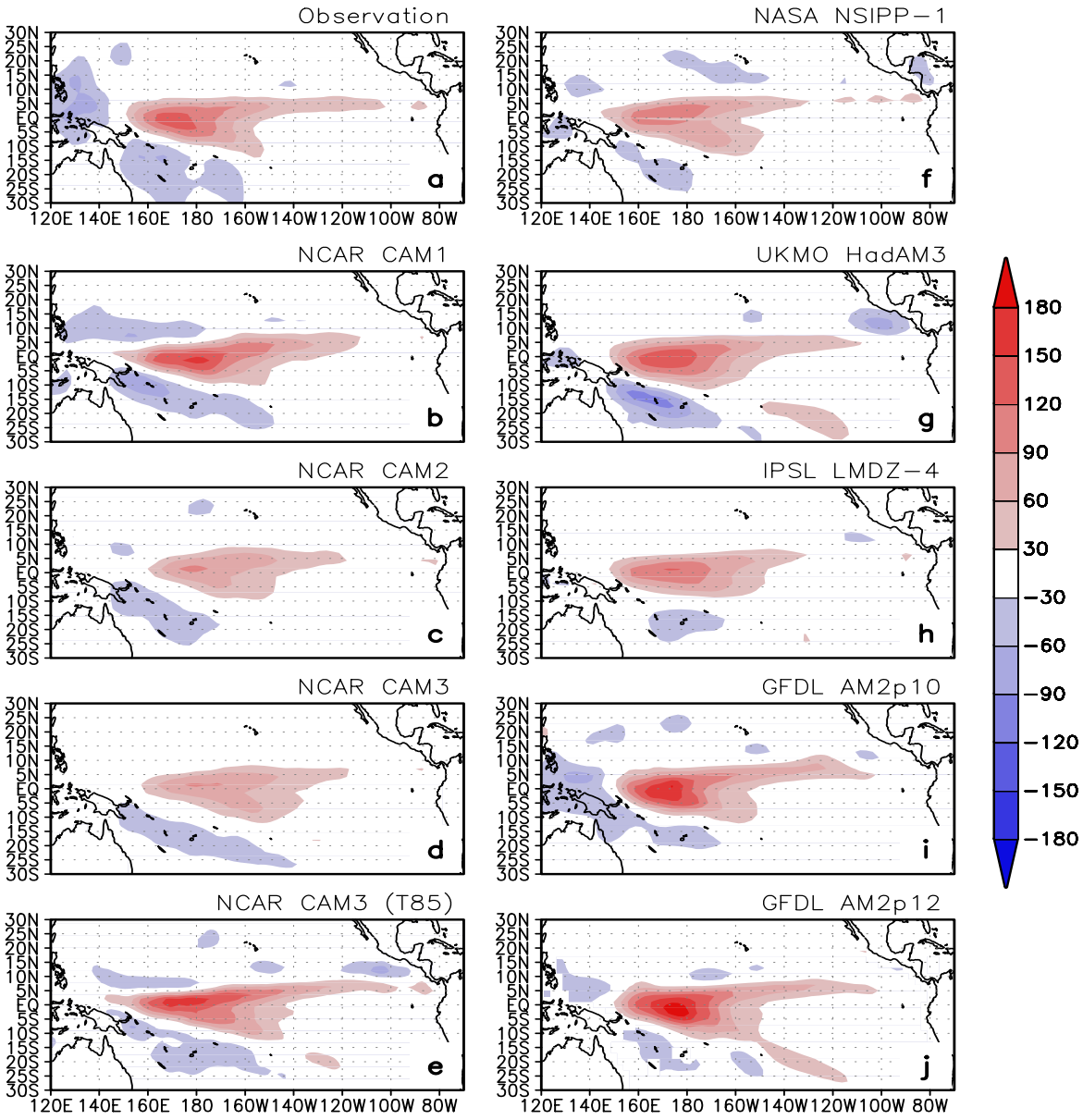

Figure 6: Response of the precipitation to El Niño warming. Shown are coefficents obtained by linearly regressing the precipitation at each grid point on the SST averaged over the equatorial Pacific (5^{O}S-5^{O}N, 150^{O}-250^{O}E). The interannual variations of the concerned quantities over the ERBE period are used for the calculations. The precipitation data are from Xie and Arkin (1996).

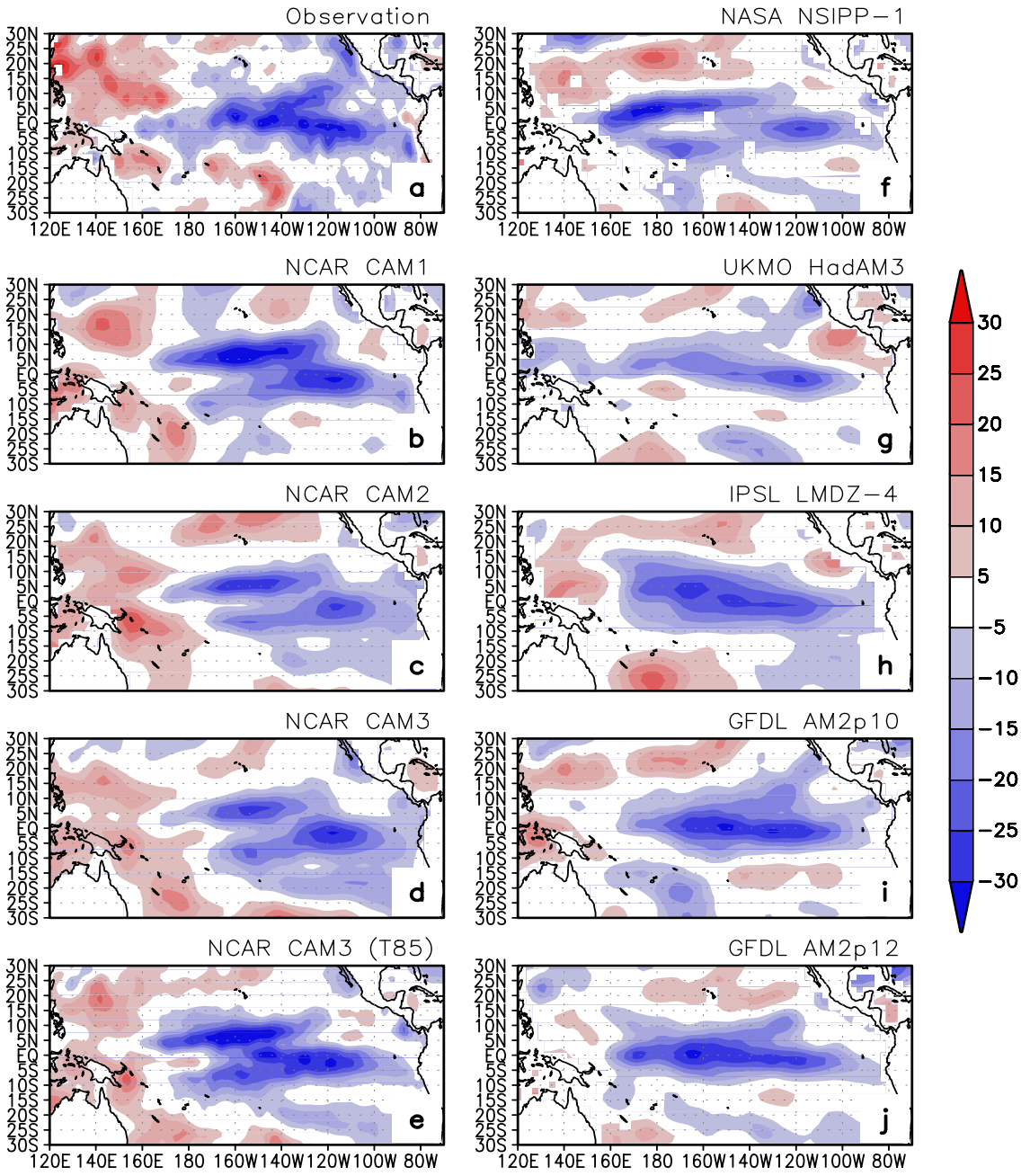

Figure 7: Response of the convergence of vertically integrated transport of energy by the atmospheric circulations (Da) to El Niño warming. Shown are coefficents obtained by linearly regressing the value of Da at each grid point on the SST averaged over the equatorial Pacific (5^{O}S-5^{O}N, 150^{O}-250^{O}E). The interannual variations of the concerned quantities over the ERBE period are used for the calculations.

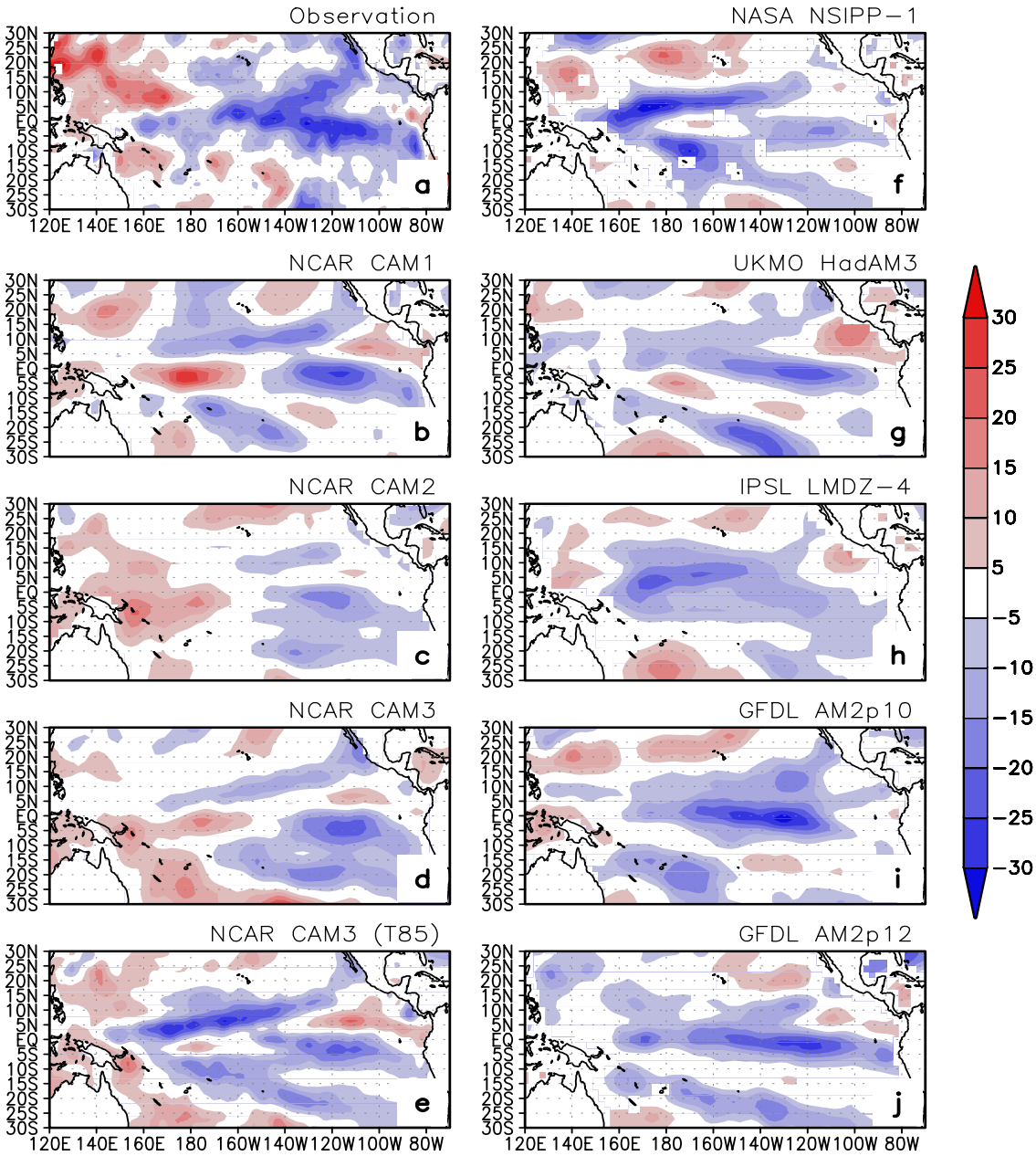

Figure 8: Response of the net surface heating (Fs) to El Niño warming. Shown are coefficents obtained by linearly regressing the net surface heating at each grid point on the SST averaged over the equatorial Pacific (5^{O}S-5^{O}N, 150^{O}-250^{O}E). The interannual variations of the concerned quantities over the ERBE period are used for the calculations. The data used for Fs are the same as in Sun et al. (2003).

Atmospheric Feedbacks in Models and Observations

Name of Process	Feedback ($Wm^{-2}K^{-1}$)									
	Observation	NCAR/CAM1	NCAR/CAM2	NCAR/CAM3	CAM3(T85)	NASA/NSIPP-1	UKMO/HadAM3	IPSL/LMDZ-4	GFDL/AM2p10	GFDL/AM2p12
$\frac{\partial(G_a)}{\partial T}$	6.72 ± 0.27	9.10 ± 0.43	8.39 ± 0.41	8.89 ± 0.39	9.69 ± 0.36	8.21 ± 0.33	10.10 ± 0.48	8.95 ± 0.35	8.08 ± 0.33	9.43 ± 0.32
$\frac{\partial(C_L)}{\partial T}$	12.21 ± 1.03	15.94 ± 1.35	6.64 ± 0.63	7.21 ± 0.72	12.63 ± 0.82	9.14 ± 0.72	7.63 ± 0.86	14.85 ± 1.08	13.52 ± 0.78	14.74 ± 0.96
$\frac{\partial(G_a + C_L)}{\partial T}$	18.93 ± 1.17	25.03 ± 1.75	15.03 ± 0.96	16.11 ± 1.06	22.31 ± 1.05	17.34 ± 1.01	17.73 ± 1.31	23.80 ± 1.35	21.61 ± 1.05	24.17 ± 1.19
$\frac{\partial(C_S)}{\partial T}$	-10.93 ± 1.37	-4.98 ± 0.60	1.87 ± 0.96	-0.56 ± 0.78	-9.72 ± 1.09	-5.95 ± 0.77	-8.94 ± 1.33	-11.77 ± 1.40	-12.74 ± 0.79	-12.58 ± 1.09
$\frac{\partial(D_a)}{\partial T}$	-16.69 ± 1.51 (-18.73 ± 1.85)	-13.63 ± 1.76	-9.18 ± 1.40	-9.02 ± 1.20	-14.34 ± 1.23	-14.08 ± 0.96	-12.11 ± 1.53	-17.70 ± 1.08	-17.63 ± 0.92	-19.40 ± 1.28
$\frac{\partial(F_A)^*}{\partial T}$	-8.69 ± 1.76	6.42 ± 1.24	7.72 ± 1.12	6.53 ± 1.00	-1.75 ± 1.23	-2.69 ± 0.97	-3.33 ± 1.64	-5.67 ± 1.14	-8.77 ± 1.12	-7.81 ± 1.53
$\frac{\partial(F_S)}{\partial T}$	-14.89 ± 1.83 (-17.03 ± 2.06)	0.44 ± 1.24	1.48 ± 1.13	0.30 ± 1.02	-8.08 ± 1.25	-8.71 ± 0.98	-9.15 ± 1.64	-11.64 ± 1.14	-14.73 ± 1.13	-13.80 ± 1.53

The net atmospheric feedback $\frac{\partial(F_A)}{\partial T} = \frac{\partial(G_a)}{\partial T} + \frac{\partial(C_L)}{\partial T} + \frac{\partial(C_S)}{\partial T} + \frac{\partial(D_a)}{\partial T}$

Table 1: Atmospheric feedbacks over the equatorial Pacific (5^{O}S-5^{O}N, 150^{O}-250^{O}E) from nine climate models. See text for the definition of the symbols for the various feedbacks. The values for these feedbacks are obtained through a linear regression using the interannual variations of the SST and the corresponding fluxes over the equatorial Pacific. The error bars are obtained using the method of Press et al. (1992) for the case in which the measurement errors of individual data points are not known. The numbers in paratheses are estimates from the ERA-40 renanalysis (the atmospheric transport Da is calculated as the difference between the net surface heat flux from the ERA-40 reanalysis and the net radiative flux at the top of the atmosphere from ERBE).